A new adaptive threshold method for FMDFB Gaussian subbands for image denoising application

E. JEBAMALAR LEAVLINE*, S. SUTHA[a], D. ASIR ANTONY GNANA SINGH[b]
Department of Electronics and Communication Engineering, Anna University, BIT Campus, Tiruchirappalli – 620 024, Tamilnadu, India
[a]*Department of Electrical and Electronics Engineering, University College of Engineering, Dindigul, Anna University, Tamilnadu, India*
[b]*Department of Computer Science and Engineering, Anna University, BIT Campus, Tiruchirappalli – 620 024, Tamilnadu, India*

Denoising is the process of mitigating the undesired noisy components present in images. This paper proposes a new subband adaptive threshold technique in FMDFB domain for noise removal. FMDFB is a multiscale perfect reconstruction filter bank structure that is efficiently used to represent images in various image processing applications including denoising. Since, the FMDFB coefficients differ from wavelet coefficients, a mere wavelet based fixed threshold will oversmooth the images. Hence, this paper proposes a subband adaptive threshold estimation scheme to determine the suitable threshold in FMDFB domain for denoising. Our experimental results depict that the proposed denoising scheme outperforms conventional multiscale denoising schemes such as wavelet and contourlet based denoising.

(Received July 19, 2015; accepted September 9, 2015)

Keywords: Image denoising, FMDFB, Wavelet transform, Adaptive threshold, SSIM

1. Introduction

Image denoising may be regarded as the process of estimating the content of interest f(x,y) from the noisy observation g(x,y) of the image. If f(x,y) be the uncorrupted image of size N×N with the spatial coordinates (x,y) and n(x,y) be the noise function, then the noisy image observation g(x,y) with additive noise is represented as shown in (1).

$$g(x,y) = f(x,y) + n(x,y) \quad \forall x,y \le N \tag{1}$$

Image denoising is a well studied area in image processing and it attracts many researchers. In spite of the state-of-the art image denoising techniques that showed considerable improvement in peak signal-to-noise ratio (PSNR), and mean square error (MSE), there is still scope for better improvement in the image quality assessment (IQA) metrics. According to Priyam Chatterjee and Peyman Milanfar [1], the MSE of the state-of-the-art methods is far higher than the estimated lower bound on MSE based on the Cramer–Rao bound [2].

Spatial domain denoising techniques process and manipulate the pixels intensities directly in the spatial domain. Most of the spatial domain filters are window/kernel based filters, and their performance relies on the size of the kernel used [3]. These filters enhance the corrupted images using the local statistics of the images as well as preserve edge shapes compared to simple mean and median filters with fixed window size. However, for homogeneous regions large window size is needed to improve noise reduction. These filters result in artefacts around the object or edge when tiny bright objects are handled resulting in roughly defined backgrounds in the neighborhood of bright edges.

On the other hand, transform domain noise removal techniques became popular because of their reduced computational complexity and efficient software and hardware implementations. Transform domain techniques work on the assumption that the true signal can be approximated well by a linear combination of few basis elements [4]. Since the clean pixels result in larger transform coefficients, shrinking the smaller coefficients will suppress the noise present in the image [5]. Starting from Fourier transform, several transform domain denoising techniques have been proposed including discrete cosine transform (DCT) based denoising [6], wavelet denoising [7] [8] and with overcomplete multiscale transforms such as ridgelet [9], curvelet [10], contourlet [11], etc.

The 2D DCT does not represent sharp transitions and singularities such as edges and contours, whereas wavelets would typically perform poorly for textures and smooth transitions [12]. Unfortunately, the enormous natural images make it impossible for any fixed 2D transform like DCT and wavelet transform to accomplish excellent sparsity [4]. The overcomplete multiscale and multiresolution transforms were proposed to overcome this problem by achieving better sparsity than the fixed wavelet transform.

Wavelet transform is effectively used in several image processing applications including denoising. Yet, the de-

noised images that result from wavelet-based denoising suffer with blocking artefacts. This is due to the fact that the separable wavelet basis functions are non-local, signal independent, and fixed shape and they are not capable of capturing and preserving significant image features such as edges and fine details [13]. Hence, multiscale and multi-resolution schemes that are highly directional with flexible basis functions and that obey orthogonal, critical sampling properties need to be used to improve the denoising performance.

Several multiscale representations such as Gabor wavelet [14], ridgelet [9], curvelet [10], steerable pyramid [15], shearlet [16], contourlet [11], etc. have been proposed in the literature. The contourlet transform, alternatively known as pyramidal directional filter banks (PDFB) was found suitable and used in various image processing applications in spite of its redundancy and computational complexity. A modification to the PDFB, namely the multiscale directional filter bank (MDFB), is designed to have fine high-frequency decomposition. The MDFB is redundant as it introduces an additional decomposition in the high-frequency band and thereby improves the radial frequency resolution at a cost of one set of extra-scale and directional decompositions on the full image size. This results in increased number of computations. In addition, MDFB has a higher redundancy than the contourlet transform. Fast and reduced redundancy structure for this MDFB (FMDFB) was proposed by Cheng et al [17]. The idea behind achieving reduced redundancy and computational complexity is that, directional decomposition on the first two scales is performed prior to the scale decomposition. This permits sharing of directional decomposition among the two scales, thus reducing the computational complexity significantly. The resultant scheme has the same redundancy as a contourlet transform and has a 33% reduction in the number of computations as compared to MDFB. Further, FMDFB exhibits perfect reconstruction. The total number of directional subband coefficients is the same as the size of the original image because of the critically sampled DFB, and hence, no extra computations are introduced by the scale decomposition.

Because of these advantages, a novel image denoising scheme with subband adaptive threshold (SAT) for FMDFB is proposed. In our earlier works, FMDFB was introduced as an image transformation scheme to aid multiscale representation of images for denoising [18]. In order to calculate the threshold value, the noisy subband selection algorithm (NSSA) was proposed in [19] to identify the highly noisy subband, based on which the threshold can be estimated. However, these algorithms use a fixed threshold for denoising. From the analysis of the FMDFB subbands, it is inferred that the magnitudes of the FMDFB coefficients are different in each subband. Hence, a subband adaptive strategy is essential to estimate the threshold value in order to achieve better denoising performance. The subband adaptive threshold is estimated based on the mathematical model of the FMDFB subband coefficients that is derived considering the statistical nature of the FMDFB subbands.

The following sections describe the modeling of FMDFB subband coefficients, image denoising scheme using FMDFB, experimental results and conclusion.

2. Mathematical modeling of FMDFB coefficients

In our earlier work, a mathematical model for FMDFB subband coefficients was derived based on the statistical properties of the subband coefficients. In this section, the inference from [20] is summarized for the ready reference to the readers. For implementation details of FMDFB, interesting readers may refer [21].

A computationally efficient and accurate model of FMDFB coefficients is needed for straightforward parameter estimation for denoising. Initially, the frequency distribution of FMDFB subbands was analyzed using the classical histogram in order to find a suitable statistical model. The goodness of fit (GoF) of the Gaussian distribution with the FMDFB subband coefficients was evaluated with the help of quantile–quantile plot (Q-Q plot) as a graphical tool. It was observed that the Q-Q plots of FMDFB subbands of clean images show that FMDFB subbands coincide with the Gaussian (normal) distribution except the tail regions. On the other hand, the FMDFB subbands of noisy images overlap with the Gaussian (normal) distribution at most of the points as shown in Fig. 1.

In order to strengthen this argument, the GoF was evaluated using the statistical tool chi-square test. The FMDFB subbands pass this test with an acceptance rate of 96.66% as summarized in Table 1. Further, the results of the GoF test are consistent even at higher noise levels. Hence, it can be concluded that the FMDFB subbands follow the Gaussian (normal) distribution with mean 'μ' and standard deviation 'σ'. Following that, the mathematical model of FMDFB coefficients was derived with the following assumptions.

Assumption1: The coefficients of any FMDFB subband are identically distributed with the same probability density function.

Assumption 2: The coefficients of FMDFB subbands of the same level of decomposition are not independent, and they are highly correlated.

Assumption 3: The coefficients of FMDFB subbands of different levels of decomposition are independent, and they are not correlated.

With a scale decomposition of *'s'* and level of directional decomposition '*l*', the FMDFB subband coefficients $\psi^{(l,s)}$ are represented as in (2) where 'γ' is the FMDFB subband.

$$\psi^{(l,s)} = \begin{cases} \{\gamma_i\}, \ i = 1,2,\ldots 2^l, \ for \ \ s = 1 \\ \{\gamma_{ij}\}, \ i = 1,2,\ldots 2^l, j = 1,2,\ldots,2^s \ for \ \ s \neq 1 \end{cases} \quad (2)$$

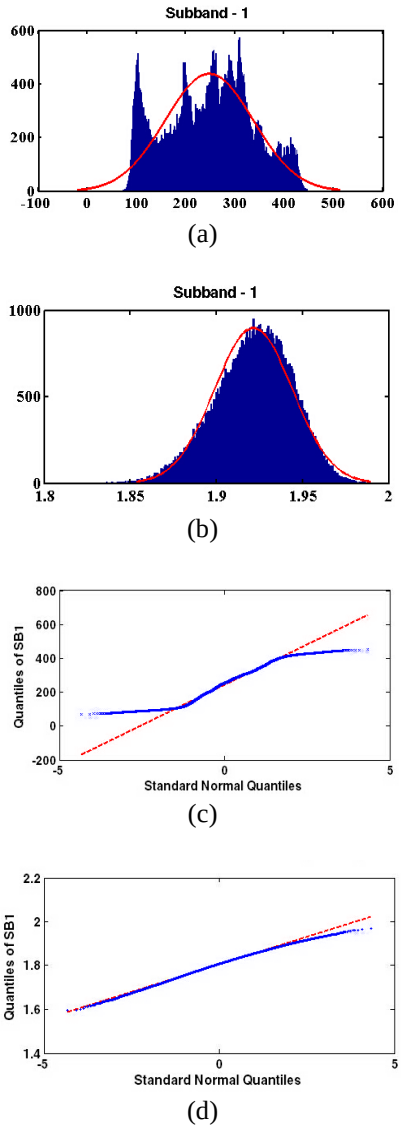

(a)

(b)

(c)

(d)

Fig. 1. (a) (b) Histogram of coefficients of sample level 1 FMDFB subband for clean and noisy (AWGN of variance 0.001) Lena image respectively (c), (d) Quantile–quantile plots showing coefficients of sample level 1 FMDFB subband for clean and noisy (AWGN of variance 0.001) Lena image respectively

The standard Gaussian (normal) distribution of a random function *'g'* follows the probability density function expressed by Equation (3) with mean μ = 0 and variance σ = 1.

$$f(g,\mu,\sigma)=\frac{1}{\sqrt{2\Pi}}e^{\frac{-g^2}{2}} \tag{3}$$

Then, the probability density function $\zeta(.)$ of the FMDFB coefficients is modeled as in Equation (4). Here, γ_{ij} are the coefficients of FMDFB subband, μ_γ is the non zero mean, and σ_γ is the standard deviation of the FMDFB subband under consideration.

$$\zeta\left(\gamma_{ij},\mu_\gamma,\sigma_\gamma\right)=\frac{1}{\sigma_\gamma\sqrt{2\Pi}}e^{\frac{(\gamma_{ij}-\mu_\gamma)^2}{2\sigma_\gamma^2}} \tag{4}$$

Table 1. Summary of GoF test results on 20 images (A – Accepted subbands, R - Rejected subbands)

Summary of GoF test of 20 images	A	R	Acceptance (%)
Clean image	385	15	96.25%
Images with Gaussian noise (zero mean & 0.001 variance)	390	10	97.5%
Images with speckle noise (0.04 variance)	385	15	96.25%

3. Image denoising using FMDFB

In this section, the subband adaptive threshold is derived and the denoising scheme using FMDFB and SAT is proposed. Further, noisy components yield smaller FMDFB coefficients and the smooth image details produce larger FMDFB coefficients similar to wavelet and contourlet coefficients. However, in FMDFB, the directional decomposition is performed only on the high frequency components of the image unlike wavelet decomposition where the lowpass image is successively decomposed into four subbands in each scale. Therefore, the directional subbands of FMDFB contain only high frequency components (noisy) and hence they are smaller in magnitude. Further, there is a higher degree of intrascale correlation and very less (near zero) interscale correlation among the FMDFB subband coefficients. So, to calculate the suitable threshold value, the noise power is estimated from the high frequency directional subbands.

3.1 Proposed subband adaptive threshold estimation for image denoising with FMDFB

This section proposes a subband adaptive threshold estimation method for FMDFB based image denoising. A distinct threshold value for each FMDFB subband is estimated from the subband statistics of the noisy image. For this purpose, the noise power in each subband is calculated with the following assumptions:

Assumption 1: The clean image 'F', the noise present in the image 'η', and the noisy image 'G' are independent of each other, they are related by $g = f + \eta$, and their variances are modeled as (5).

$$\sigma_g^2=\sigma_f^2+\sigma_\eta^2 \tag{5}$$

where σ_g^2, σ_f^2, and σ_η^2 are the variance of noisy image, clean image, and noise present in the image, respectively.

Assumption 2: The coefficients of any FMDFB subband are identically distributed with the same probability density function.

Assumption 3: The coefficients of FMDFB subbands of the same level of decomposition are not independent and they are highly correlated.

Assumption 4: The coefficients of FMDFB subbands of different levels of decomposition are independent, and they are not correlated.

The proposed subband adaptive threshold is estimated as follows.

Let *'s'* be the number of scale decompositions and *'l'* be the number of directional decompositions. SB_{pq} denotes the FMDFB subbands of size M×N at scale 's_i' where s_i=1,2,…,s. Then, $\sigma^2_{g(p,q)}$ is estimated using Equation (6) where '*p*' and '*q'* represent the subband index p=1,2,…,2^l and q=1,2,…,2^s.

$$\hat{\sigma}^2_{g(p,q)} = \frac{1}{M \times N} \sum_{i,j=1}^{M,N} [SB_{(p,q)}(i,j)]^2 \tag{6}$$

where $\hat{\sigma}^2_g$ is the estimated variance of noisy image. The noise power $\sigma^2_{\eta(p,q)}$ in each subband SB_{pq} is calculated as in (7).

$$\sigma^2_{\eta(p,q)} = \alpha \frac{median\left(\left|SB_{(p,q)}(i,j)\right|\right)}{0.675} \tag{7}$$

The scaling parameter *'α'* is calculated from the subband statistics. At the finest scale *'s'* the subband noise power is calculated for each subband SB_{pq} as expressed in (8) and (9).

$$VAR(SB_{pq}) = \frac{1}{M \times N} \sum_{i,j=1}^{M,N} [SBpq(i,j) - \overline{SB}pq]^2 \tag{8}$$

$$\overline{SB}_{pq} = \frac{1}{M \times N} \sum_{i,j=1}^{M,N} SB_{pq}(i,j) \tag{9}$$

where VAR(SB_{pq}) is the variance of the subband SB_{pq}.

Then, the scaling parameter *'α'* is calculated using (10) and the subband adaptive threshold (SAT) for FMDFB is derived as 'T_{FMDFB_SAT}' is calculated using Equation (11).

$$\alpha = \max\{VAR(SB_{pq})\} \tag{10}$$

$$T_{FMDFB\_SAT} = \frac{\hat{\sigma}^2_\eta}{\hat{\sigma}_{f(p,q)}} \tag{11}$$

$$\because \quad \hat{\sigma}_{f(p,q)} = \sqrt{\max\left(\hat{\sigma}^2_g - \hat{\sigma}^2_\eta\right), 0}$$

where σ^2_G, σ^2_F, and σ^2_η are the variances of noisy image, clean image, and the noise present in the image, respectively. This 'T_{FMDFB_SAT}' can be applied using the soft threshold method to shrink the noisy FMDFB subband coefficients.

3.2 Denoising images using FMDFB

The denoising using FMDFB with SAT undergoes the following steps.

Step 1: Read the noisy image

Step 2: Set the number of scale (*s*) and directional (*l*) decompositions

Step 3: Perform FMDFB decomposition and obtain $2^s \times 2^l$ subbands.

Step 4: Apply NSS algorithm [19] to identify the noisy subband.

Step 5: Estimate the threshold for each subband using (11).

Step 6: Apply the estimated threshold for each subband using soft threshold approach.

Step 7: Perform FMDFB reconstruction using the inverse FMDFB structure.

Step 8: Obtain the denoised image.

Step 9: Evaluate the denoising performance in terms of image quality assessment metrics.

3.3 Denoising colour images

The proposed FMDFB-based denoising is also suitable for colour image denoising. The procedure of colour image denoising based on RGB colour model is as follows. First, the colour image is split into red, green and blue colour planes. Then, FMDFB decomposition is performed on each colour plane followed by the estimation of threshold value.

The FMDFB coefficients are then shrinked by soft thresholding technique. Then, each colour plane is reconstructed using the synthesis FMDFB filter structure. Finally, the colour planes are combined to form the de-noised colour image. Further, to reduce the time complexity incurred in processing colour images, the proposed algorithm is employed with HSI (Hue Saturation Intensity) colour model. With HSI model, the denoising is performed only in the intensity plane while keeping the saturation and intensity planes unaltered. Nonetheless, before HSI and FMDFB decomposition the image needs to be converted from RGB to HSI model.

4. Experimental results and discussion

4.1 Experimental setup

The experiments were carried out with MATLAB 7.5.0 (R2007b) on a set of standard gray scale and colour

images of sizes 256×256, 512×512 and1024×1024. The number of DFB levels is chosen as 2, and two stages of decomposition are performed. For simulation purpose, noisy image is generated with the MATLAB image processing tool box function *imnoise*, at various noise variances with zero mean following normal probability distribution. In our experiments, we attempt to remove Gaussian noise using the proposed algorithm. The experiments were carried out with the work station specification of Intel(R) Core(TM) i3 CPU M330 @2.13GHz, 3.00Gb RAM, and 32-bit Windows 7 home premium operating system. The performance of the proposed FMDFB+SAT denoising algorithm is evaluated in terms of the image quality assessment metrics such as mean square error (MSE), peak signal-to-noise ratio (PSNR), structural similarity index (SSIM), and feature similarity index (FSIM).

4.2 Discussion

The proposed subband adaptive threshold (SAT) for FMDFB performs better for Gaussian noise removal application. Table 2 compares SSIM and FSIM values of wavelet denoising, contourlet denoising, denoising with FMDFB+NSSA, and denoising using FMDFB+SAT. The experimental results show that image denoising using FMDFB+SAT outperforms the methods compared. Furthermore, from Table 3 it is obvious that the proposed denoising scheme using FMDFB with SAT takes less time than contourlet-based denoising. However, it takes more time than the wavelet-based denoising. Another exciting fact is that the computation time depends on the length of the FIR filters used to realize the FMDFB filter bank structure. The proposed image denoising algorithms namely FMDFB+SAT tends to preserve the fine details of the images when compared to wavelet and contourlet-based image denoising as it is evident from Fig. 2.

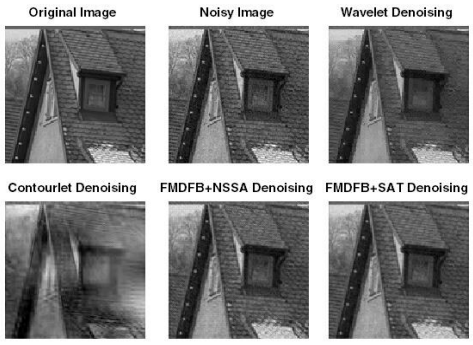

Fig. 2. Performance of denoising algorithms on gray scale image (cropped houses) degraded with zero mean additive white Gaussian noise with variance 0.001 (with FSIM of 0.9355, 0.8299, 0.8997, and 0.9412 for wavelet, contourlet, FMDFB + NSSA, and FMDFB + SAT respectively)

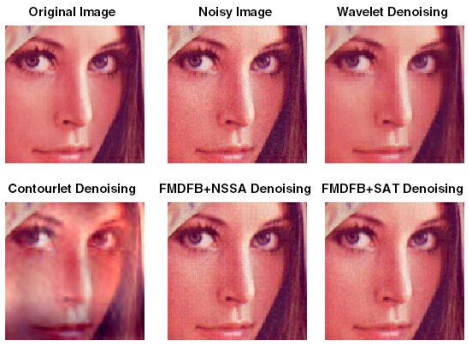

Fig. 3. Performance of proposed denoising algorithms on colour images (cropped Lena image) degraded with zero mean additive white Gaussian noise with variance 0.001 (with FSIM of 0.9264, 0.8591, 0.9195, and 0.9295 for wavelet, contourlet, FMDFB + NSSA, and FMDFB+SAT respectively).

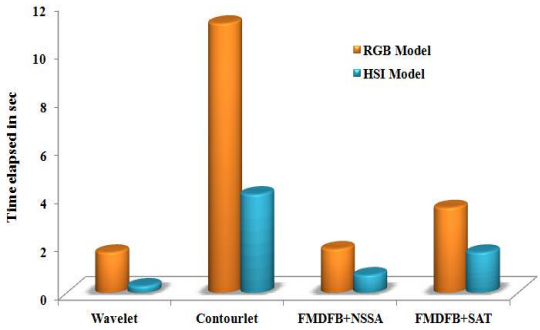

Fig. 4. Comparison of average time elapsed in seconds using RGB and HSI colour models

From Fig. 3 and Table 4, it is evident that the denoising performance of the proposed algorithm on colour images is consistent with gray scale image denoising in terms of IQA metrics and computation time. With HSI colour model, the time complexity is reduced more that 60% for fixed image size as shown in Figure 4. The wavelet based denoising takes less time when compared to contourlet and the proposed denoising methods as in the case of RGB colour model. However, similar denoising performance is achieved using RGB and HSI colour models.

Further the following facts are observed from the denoised images. The images resulting from wavelet based denoising has some visible artefacts. Contourlet denoising preserves edges compared to wavelet denoising, but the structural information is not maintained up to the desired level. Also, the inherent computational complexity is higher than that of wavelet denoising. FMDFB+NSSA performs better than contourlet denoising; however the denoised images lose edge details because of the fixed global threshold adopted. The images denoised with FMDFB+SAT are appealing visually as well as in terms of image quality assessment methods compared.

The subband adaptive threshold (SAT) takes the FMDFB subband statistics into consideration and calculates different threshold value for each FMDFB subband.

This is due to the fact that fixed global threshold value may degrade the denoising performance by over smoothing as the FMDFB subbands at the finer scale differ in magnitude even though they follow Gaussian distribution. SAT preserves details better than the fixed global threshold. The visible artefacts resulting from wavelet denoising are considerably minimized by this algorithm.

5. Conclusions and future work

This paper proposed a new subband adaptive threshold (SAT) estimation based on the FMDFB subband for image denoising. The visual artefacts resulting from wavelet-based denoising because of its fixed basis are effectively handled by the FMDFB-based denoising proposed in this work. The threshold value is estimated considering the statistical nature of the FMDFB subbands in MATLAB environment. The proposed denoising scheme namely FMDFB+SAT is appealing both visually and quantitatively. This is due to the fact that FMDFB is a perfect reconstruction framework that is highly local and directional. The filter components of FMDFB are carefully designed so as to avoid aliasing effect and maintain good frequency resolution. Hence, it preserves the fine details of the image such as edges. In addition, the application of the proposed denoising algorithms is extended to colour images. The experimental results of colour image denoising are consistent with that of grayscale images. Further, the time complexity of the algorithms compared was also studied. Also the time complexity of denoising colour images is reduced by adopting HSI colour model.

In future, the estimated threshold value can be optimized for a particular subband using intelligent optimization techniques. Further, it is possible to increase the scale and directional decomposition levels. This would aid the analysis of noisy components that are attributed to high frequency with finer frequency resolution in applications such as image analysis.

Table 2. Comparison of SSIM and FSIM of wavelet denoising, contourlet denoising, denoising with FMDFB+NSSA, and denoising with FMDFB+SAT for grayscale images degraded with zero mean additive white Gaussian noise with variance 0.001

Image	Wavelet denoising		Contourlet denoising		FMDFB+ NSSA		FMDFB+ SAT	
	SSIM		FSIM		SSIM		FSIM	
Aerial	0.85	0.92	0.67	0.86	0.82	0.92	0.89	0.95
Airfield	0.92	0.96	0.62	0.80	0.95	0.98	0.96	0.98
Barbara	0.86	0.92	0.57	0.81	0.81	0.91	0.86	0.93
Boat	0.83	0.92	0.60	0.83	0.80	0.91	0.86	0.94
Bridge	0.85	0.90	0.53	0.81	0.84	0.92	0.89	0.94
Cameraman	0.80	0.92	0.52	0.74	0.73	0.89	0.82	0.91
Goldhill	0.82	0.91	0.53	0.81	0.82	0.92	0.87	0.93
Houses	0.91	0.93	0.60	0.82	0.80	0.89	0.86	0.94
Lake	0.84	0.92	0.46	0.78	0.81	0.92	0.87	0.94
Lena	0.81	0.92	0.66	0.85	0.79	0.92	0.86	0.93
Lighthouse	0.84	0.92	0.49	0.81	0.76	0.89	0.84	0.93
Livingroom	0.85	0.92	0.61	0.84	0.81	0.92	0.87	0.94
Mandrill	0.84	0.90	0.61	0.83	0.80	0.91	0.86	0.94
Monarch	0.84	0.93	0.68	0.84	0.80	0.90	0.85	0.93
Peppers	0.81	0.92	0.56	0.81	0.81	0.92	0.86	0.94
Tulips	0.86	0.91	0.52	0.79	0.85	0.90	0.89	0.93
Zelda	0.81	0.92	0.64	0.85	0.83	0.92	0.87	0.93
Zoneplate	0.95	0.91	0.94	0.89	0.75	0.86	0.95	0.97

Table 3. Comparison of average time elapsed for wavelet denoising, contourlet denoising, denoising with FMDFB+NSSA, and denoising with FMDFB+SAT with pyramidal filter '9/7' and directional filter 'pkva'

Image size	Time elapsed in seconds			
	Wavelet denoising	Contourlet denoising	FMDFB+ NSSA	FMDFB+ SAT
256×256	0.1951	1.3651	0.1916	0.5256
512×512	0.2742	3.8311	0.6188	1.2417
1024×1024	0.6669	13.772	2.4315	3.8145

Table 4. Comparison of SSIM and FSIM of wavelet denoising, contourlet denoising, denoising with FMDFB+NSSA, and denoising with FMDFB+SAT for colour images degraded with zero mean additive white Gaussian noise with variance 0.001

Image	Wavelet de-noising		Contourlet de-noising		FMDFB+NSSA		FMDFB+SAT	
	SSIM	FSIM	SSIM	FSIM	SSIM	FSIM	SSIM	FSIM
Fruits	0.80	0.91	0.55	0.79	0.76	0.91	0.84	0.92
Kp07	0.85	0.92	0.65	0.83	0.80	0.91	0.86	0.94
Kp21	0.82	0.92	0.60	0.83	0.74	0.90	0.82	0.93
Lena	0.80	0.92	0.69	0.85	0.78	0.91	0.85	0.92
Mandrill	0.84	0.91	0.51	0.79	0.80	0.91	0.87	0.94
Monarch	0.84	0.93	0.65	0.83	0.80	0.91	0.85	0.93
Peppers	0.80	0.92	0.53	0.80	0.79	0.91	0.85	0.93
Sails	0.86	0.91	0.61	0.85	0.81	0.90	0.86	0.93
Tulips	0.86	0.91	0.49	0.77	0.84	0.90	0.89	0.93

References

[1] P. Chatterjee, P. Milanfar, IEEE Trans. Image Process. 895 (2010).
[2] Y. C. Eldar, Found. Trends Signal Process. 305 (2008).
[3] R. C. Gonzalez, R. E. Woods, S. L. Eddins, Digital image processing using MATLAB, Up. Saddle River NJ Jensen Prentice Hall (2004).
[4] K. Dabov, A. Foi, V. Katkovnik, K. Egiazarian, IEEE Trans. Image Process. 2080 (2007).
[5] S. Sutha, E. Jebamalar Leavline, D. Asir Antony Gnana Singh, WSEAS Trans. Signal Process. 203 (2014).
[6] A.Foi, V.Katkovnik, K.Egiazarian, IEEE Trans. Image Process. 1395 (2007).
[7] K. P. Soman, K. I. Ramachandran, N. G. Resmi, PHI Learning Pvt. Ltd., (2010).
[8] M. K. Mıhçak, I. Kozintsev, K. Ramchandran, Proc. IEEE International Conference on Acoustics, Speech, and Signal Processing, 1999, p. 3253.
[9] G. Y. Chen, B. Kégl, Pattern Recognit., 578 (2007).
[10] J.-L.Starck, E.J Candes, D.L.Donoho, IEEE Trans. Image Process.670 (2002).
[11] M. N. Do, M. Vetterli, IEEE Trans. Image Process. 2091 (2005).
[12] D. D. Y. Po, M. N. Do, IEEE Trans. Image Process. 1610 (2006).
[13] M. N. Do, M. Vetterli, IEEE Trans. on Signal Process. 2329 (2003).
[14] O. Nestares, A. Tabernero, R. Navarro, J. Portilla, J. Electron. Imaging. 166 (1998).
[15] H. Rabbani, Pattern Recognit. 2181 (2009).
[16] W.Q.Lim, IEEE Trans. Image Process. 1166 (2010).
[17] K.O. Cheng, N.-F. Law, W.-C. Siu, IEEE Trans. on. Image Process. 2058 (2007).
[18] E. J. Leavline, S. Sutha, D. A. A. G. Singh, J. Opt. Soc. Am. A. 283 (2014).
[19] S. Sutha, E. J. Leavline, D. A. A. G. Singh, Inf. Technol. J. 1289 (2013).
[20] E. J. Leavline, S. Sutha, J. Mod. Appl. Stat. Methods., to be published.
[21] E. J. Leavline, S. Sutha Int. J. U- E-Serv. Sci. Technol. 221 (2014).

*Corresponding author: jebi.lee@gmail.com